Quantum effects in the transport properties of nanoelectronic three-terminal Y-junction devices

Dan Csontos* and H. Q. Xu†
Solid State Physics, Lund University, P.O. Box 118, SE-221 00 Lund, Sweden
(Received 3 February 2003; published 23 June 2003)

We report on a theoretical study of the electrical properties of three-terminal ballistic junction (TBJ) devices, consisting of three perfect leads and a ballistic coupling region, using a multiterminal scattering-matrix approach and the Landauer-Büttiker transport theory. The calculations have been performed for TBJ devices with different structure properties, at both high and low temperatures, as well as at both small and large applied bias voltages. The study is focused on the effects of quantum scattering, which is treated by exact numerical calculations. It is shown that when operated in the push-pull fashion, i.e., by applying finite voltages $V_l = V$ and $V_r = -V$ to the left and right branches, the TBJ devices exhibit strong nonlinearities in the output voltage V_c calculated at the central branch. At high temperatures, the output voltage V_c as a function of V shows the same nonlinear characteristics as observed in recent theoretical analyses and experimental measurements. These high-temperature electrical characteristics are found to be qualitatively insensitive to the structure details of the devices and reveal little effect of quantum scattering. At low temperatures, the output voltage V_c shows fluctuations, and can assume either negative or positive values, depending on the chemical potential, at small bias regions. These behaviors are explained in terms of the fluctuations seen in the transmissions between the terminals, while the transmission fluctuations are shown to arise from strong scattering by quasibound states formed in the junction cavity region and are therefore signatures of quantum effects. Based on the quantum fluctuation nature of the device characteristics, a single multilogic device, constructed with a single TBJ, with switching of the logic functions by means of a gate, is proposed.

DOI: 10.1103/PhysRevB.67.235322 PACS number(s): 73.23.Ad, 73.63.Rt, 85.35.Ds

I. INTRODUCTION

Rapid advances in nanoelectronic fabrication techniques have, in recent years, made possible the realization of electron waveguide devices with dimensions smaller than the elastic and inelastic scattering lengths of the conduction electrons. Based on the ballistic and phase-coherent natures of the electron transport, various interesting nanoelectronic devices, such as the directional coupler,[1] the quantum stub transistor,[2] and the three-terminal ballistic junction (TBJ),[3–10] have been proposed. In particular, the Y-shaped TBJ, also known as the Y-branch switch, was proposed as a promising alternative for future low-power, high-speed switching devices.[3] In such a device, electrons injected from a source contact are deflected by a lateral electric field, created by gates in the branching region, into either of the two drain contacts.

Very recently, a different type of functionality of TBJ devices, revealing new and interesting nonlinear transport phenomena, was theoretically proposed[7] and experimentally demonstrated.[8–10] It was shown that when finite voltages V_l and V_r are applied in the push-pull fashion, with $V_l = V$ and $V_r = -V$, to the left and right branches of a symmetric TBJ device, the output voltage V_c measured at the central branch is always negative. This property was observed in both Y-shaped[8,10] and T-shaped[9] TBJs, suggesting that the observed phenomena are inherent to TBJs in general. The origins of the observed transport phenomena were analyzed by Xu[7] using the Landauer-Büttiker transport theory.[11] In this analysis, the TBJs were modeled by three saddle-point[12] contacts connected via a ballistic cavity with adiabatic boundaries, thus neglecting the effects of electron scattering in the junction cavity region. The analysis showed that, indeed, for a symmetric TBJ of arbitrary shape operating in the push-pull fashion, the output voltage V_c from the central branch is negative, monotonically decreasing as a function of $|V|$. Furthermore, it was also shown that these characteristics are present also for devices with broken symmetry, provided that $|V|$ is greater than a certain threshold. Promising applications of TBJ devices in nanoelectronics, such as rectification, second-harmonic generation and logic function, were proposed[7,13,14] and have been demonstrated experimentally.[15] In addition, very recently, based on the single, planar nature of the device structure, the fabrication of TBJs using nanoimprint lithography on high-quality semiconductor heterostructures has been demonstrated,[16] giving possibility for future mass production of these devices.

A natural and interesting extension of the analysis of Ref. 7 is to consider also the effects of electron scattering in the junction region. In TBJ devices, the conduction electrons can experience scattering caused by, e.g., abrupt changes in the geometry and potential profile, complicated shapes of the TBJs, as well as impurity and boundary roughness (the latter caused by, e.g., the process of etching[17]). In particular, the central coupling junction of a TBJ may become a source of strong electron scattering as a result of the formation of quasibound states. Such a quantum effect of ballistic cavities was previously studied in two-terminal setups, for which the electron transport was found to show strong signatures of quantum scattering and interference.[18–21]

In this work, we present a numerical study of the electrical properties of TBJ devices with realistic structure boundaries based on a formalism in which quantum-mechanical scattering of electrons is fully included.[22] Various TBJ devices with different shapes and sizes of the ballistic cavity and of the connecting waveguides have been studied. The

 ©2003 The American Physical Society

electric characteristics of the devices in both the linear- and the nonlinear-response regimes of transport have been calculated. Furthermore, the temperature dependence of the observed features has been investigated.

In the nonlinear-response regime of transport, the study has been focused on the analysis of the push-pull operation of symmetric and asymmetric TBJ devices made from III–V semiconductor materials with characteristic feature sizes around 100 nm. We have found that at high temperatures, the TBJ devices, when operated in the push-pull fashion, exhibit the same electrical characteristics as in Refs. 7–10. We have also found that these high-temperature characteristics are qualitatively insensitive to the structure details of the devices and reveal little effect of quantum scattering, which supports the assumption made in Ref. 7. At low temperatures, however, it is found that the output voltage V_c from the central branch of the TBJs can exhibit fluctuations and can, depending on the chemical potential, assume either positive (even for a symmetric TBJ) or negative values at small bias voltages. Thus, a single TBJ structure may be used as a multilogic device with switching of the logic functions by tuning the chemical potential using a gate.

The quantum-mechanical origin of the low-temperature characteristics of the TBJ were further studied by transport calculations in the linear response regime. We have found that in the absence of scattering, the transmissions between the left (right) and the central branches of the symmetric TBJ devices show unit or half-unit quantization steps depending on the size of the three leads. For structures in which a cavity is formed at the junction between the three branches, fluctuations on top of the transmission steps, resulting from scattering by quasibound states formed in the cavity region, are observed. The details of the features are found to depend strongly on the geometrical design of the devices.

The rest of the paper is organized as follows. In Sec. II, we will give a brief overview of the method used in our analyses. In Sec. III, we will first present the model of the device used in this work, and then show and discuss the results of the calculations for the transmissions and the push-pull nonlinear operation of symmetric and asymmetric TBJs at two characteristic temperatures. A demonstration of multilogic functionality will also be presented and discussed in this section. The paper is concluded in Sec. IV.

II. THEORETICAL MODEL

The formalism used in the numerical calculations has been described elsewhere,[22] and only a brief overview will be given in the following. In short, the method consists of an implementation of the scattering-matrix method[23–26] for three-terminal Y-junction devices, from which the transmissions and reflections of electrons between the three terminals can be obtained in terms of the scattering-matrix of the system.

Any type of potential profile can be treated by dividing the system into thin segments along the x direction of transport, which are thin enough such that the potential in each segment can be assumed to be of transverse dependence only (see Fig. 1 for schematics). The wave function of an electron

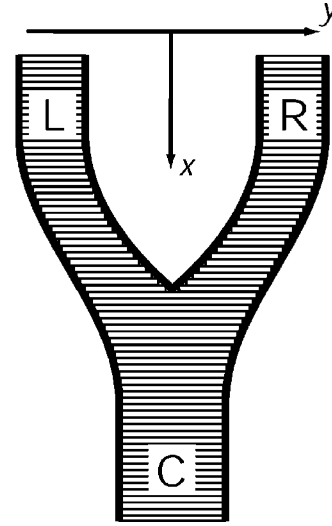

FIG. 1. Schematics of a three-terminal Y-branch device. The modeling of the TBJ is done by dividing the device into thin segments along the x direction, which are thin enough such that the potential profile in each segment is of transverse (y) dependence only.

with energy ε in an arbitrary segment labeled i of lead b (where $b=l,r,c$ labels the three, i.e., left, right, and central, branches/arms) satisfies the following Schrödinger equation:

$$H\Psi^{b,i}(x,y)=\varepsilon\Psi^{b,i}(x,y), \quad (1)$$

with the Hamiltonian H given by

$$H=-\frac{\hbar^2}{2m^*}\left(\frac{\partial^2}{\partial x^2}+\frac{\partial^2}{\partial y^2}\right)+U_c^{b,i}(y)+U_s^{b,i}(y), \quad (2)$$

where $U_c^{b,i}(y)$ describes the transverse confinement defined by the boundaries of the TBJ (thick solid lines in Fig. 1), $U_s^{b,i}(y)$ is the transverse potential inside the segment, and m^* is the effective mass of the electron. Expanding the wave function $\Psi^{b,i}(x,y)$ in terms of a complete set of basis functions $\{\psi_\beta^b(y)\}$ with eigenvalues $\{\epsilon_\beta^b\}$ in branch b (Refs. 22, 24) gives

$$\Psi^{b,i}(x,y)=\sum_\alpha \psi_\alpha^b(y)\sum_n d_{\alpha n}^{b,i}[a_n^{b,i+}e^{\mathrm{i}k_n^{b,i}(x-x_0^{b,i})} + a_n^{b,i-}e^{-\mathrm{i}k_n^{b,i}(x-x_0^{b,i})}], \quad (3)$$

where $x_0^{b,i}$ is a reference coordinate in segment i along the x direction and $k_n^{b,i}=[2m^*(\varepsilon-E_n^{b,i})/\hbar^2]^{1/2}$ are longitudinal wave numbers which may be either real or imaginary, thus corresponding to propagating or evanescent states, respectively. The label $+$ $(-)$ denotes a state that is propagating forward or evanescent (propagating backward or exponentially increasing). The expansion coefficients $\{d_{\alpha n}^{b,i}\}$ and transverse eigenvalues $\{E_n^{b,i}\}$ can be obtained from the following system of equations:

$$\sum_{\alpha}\left[(\epsilon_{\beta}^{b}-E_{n}^{b,i})\delta_{\beta\alpha}+\langle\psi_{\beta}^{b}(y)|U_{T}^{b,i}(y)|\psi_{\alpha}^{b}(y)\rangle\right]d_{\alpha n}^{b,i}=0,$$

$$\beta=1,2,3,\ldots, \tag{4}$$

where $U_T^{b,i}(y)=U_c^{b,i}(y)+U_s^{b,i}(y)$.

The unknowns remaining to be found are the coefficients $\{a_n^{b,i\pm}\}$. We have previously shown[22] that the coefficients for the outermost segments of a TBJ (serving as perfect, semi-infinite leads) can be related via a three-terminal scattering matrix $\mathbf{S}(l,r,c)$ according to the follwing relation:

$$\begin{pmatrix}\mathbf{A}^{c+}\\ \mathbf{A}^{r-}\\ \mathbf{A}^{l-}\end{pmatrix}=\mathbf{S}(l,r,c)\begin{pmatrix}\mathbf{A}^{r+}\\ \mathbf{A}^{l+}\\ \mathbf{A}^{c-}\end{pmatrix}, \tag{5}$$

where $\mathbf{A}^{l\pm}$, $\mathbf{A}^{r\pm}$, and $\mathbf{A}^{c\pm}$ are column vectors containing the coefficients $\{a_n^{l\pm}\}$, $\{a_n^{r\pm}\}$, and $\{a_n^{c\pm}\}$ in the outermost segments, i.e., the lead portions of the three branches, respectively. The scattering matrix $\mathbf{S}(l,r,c)$ can be used for the calculation of the transmission and reflection characteristics of the TBJ. For example, the probability that an electron incident with energy ε, in state m from lead b, to be transmitted to state n in lead b' is given by

$$T_{b'b}^{nm}=\frac{k_n^{b'}}{k_m^{b}}|(\mathbf{S}_{b'b})_{nm}|^2, \tag{6}$$

where $k_n^{b'}$ and k_m^{b} are the wave vectors in the leads b' and b, respectively, and $\mathbf{S}_{b'b}$ is a submatrix of the scattering matrix $\mathbf{S}(l,r,c)$, which is defined by rewriting Eq. (5) as

$$\begin{pmatrix}\mathbf{A}^{c+}\\ \mathbf{A}^{r-}\\ \mathbf{A}^{l-}\end{pmatrix}=\begin{bmatrix}\mathbf{S}_{cr} & \mathbf{S}_{cl} & \mathbf{S}_{cc}\\ \mathbf{S}_{rr} & \mathbf{S}_{rl} & \mathbf{S}_{rc}\\ \mathbf{S}_{lr} & \mathbf{S}_{ll} & \mathbf{S}_{lc}\end{bmatrix}\begin{pmatrix}\mathbf{A}^{r+}\\ \mathbf{A}^{l+}\\ \mathbf{A}^{c-}\end{pmatrix}. \tag{7}$$

At zero temperature, the total transmission between the two branches b and b' at a given energy ε is given by

$$T_{b'b}(\varepsilon)=\sum_{n,m}^{(occ)}\frac{k_n^{b'}}{k_m^{b}}|(\mathbf{S}_{b'b})_{nm}|^2, \tag{8}$$

where the summation is performed over all occupied states. At finite temperature T, we define the total transmission according to

$$T_{b'b}(\mu_F,T)=\int_0^{\infty}T_{b'b}(\varepsilon)\left[-\frac{\partial f(\varepsilon-\mu_F,T)}{\partial\varepsilon}\right]d\varepsilon, \tag{9}$$

where $f(\varepsilon-\mu_F,T)$ is the Fermi distribution function and μ_F is the chemical potential of the device at zero bias. The reflection of electrons into the same lead is defined by $R_{bb}(\mu_F,T)=T_{bb}(\mu_F,T)$.

Here, we note that in the formulation, Eq. (4) should consist of an infinite number of coupled equations, corresponding to an infinite-order wave function expansion in Eq. (3). In calculations, however, Eq. (4) has to be solved numerically by truncating the number of basis functions at a high transverse level M_b. In this work, we set M_b for each branch as large as it is necessary, i.e., we include all propagating modes and a necessarily large number of evanescent modes to obtain the desired convergence in the transmissions.

The nonlinear transport properties of the device can also be calculated from the transmissions $T_{b'b}(\varepsilon)$. As stated in the Introduction, we are interested in the calculations of the output voltage V_c from the floating central branch, when finite voltages V_l and V_r are applied in the push-pull fashion, i.e., with $V_l=V$ and $V_r=-V$, to the left and right branches of the TBJ. The current in the central branch can be calculated from[7,11]

$$I_c=\frac{2e}{h}\left\{\int[N_c(\varepsilon)-R_{cc}(\varepsilon)]f(\varepsilon-\mu_c,T)d\varepsilon-\sum_{i=l,r}\int T_{ci}(\varepsilon)f(\varepsilon-\mu_i,T)d\varepsilon\right\}, \tag{10}$$

where N_c is the number of current-carrying modes in the central lead, and $\mu_l=\mu_F-eV$ and $\mu_r=\mu_F+eV$ are electrochemical potentials in the left and right reservoirs, respectively. The output voltage V_c can be calculated from $eV_c=-(\mu_c-\mu_F)$, where the electrochemical potential μ_c, can be obtained from Eq. (10) by requiring $I_c=0$. In principle, the transmissions T_{cl} and T_{cr}, and the reflection R_{cc} are functions of the applied voltages V_l and V_r. However, it has been shown that most of the resistance in a ballistic device is due to the contacts.[27] Thus, in the present calculations, the electrostatic potential is assumed to be flat within the TBJ structure, and the voltage drops are assumed to occur only at the three contacts. These assumptions lead to the simplified expression of Eq. (10) for the current I_c, which depends on the applied voltages only through the Fermi function.

III. RESULTS AND DISCUSSION

In the following, we will first briefly describe the model TBJs used in our calculations. We then present and discuss the results of our calculations, which we have performed for both symmetric and asymmetric TBJs at low and high temperatures and in the linear and nonlinear regimes of transport. For the nonlinear transport properties, we restrict our investigation to the previously mentioned push-pull operation, i.e., applying bias voltages $V_l=-V_r=V$ to the left and right branches of the TBJ, while calculating the output voltage V_c obtained by requiring $I_c=0$. The results are accompanied by spectra of the transmissions between the three leads, which are used for understanding the details of the observed nonlinear transport characteristics.

A. Device model

Numerical calculations have been performed for a number of Y-shaped TBJs, consisting of three electron waveguides and a ballistic coupling region. In the calculations, the hard-wall confinement potential has been used in order to constrain the electron motion within the TBJ. The effective mass m^* was chosen to be $m^*=0.047m_0$, which corresponds to

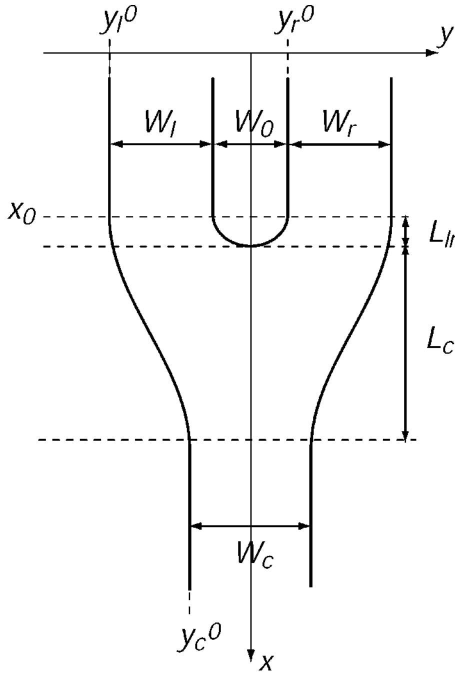

FIG. 2. Schematics of a TBJ device as modeled in the calculations.

the GaInAs system used in the experiments by Hieke and Ulfward[8] and by Shorubalko *et al.*[9]

Figure 2 shows a model of the Y-shaped TBJs considered in the present paper. The shape and size of the TBJs have been defined by introducing a few characteristic geometrical parameters W_l, W_r, W_c, W_0, L_c, and L_{lr} $(=W_0/2)$, and by describing the structure boundaries by analytical formulas. In terms of the parameters, shown in Fig. 2, the transverse positions of the outer boundaries of the TBJs vary within the region $x_0<x<x_0+L$, where $L=L_{lr}+L_c$, according to

$$y_l^{out}(x)=\frac{y_c^0+y_l^0}{2}+\frac{y_c^0-y_l^0}{2}\sin\left(\frac{x-x_0}{L}\pi-\frac{\pi}{2}\right),$$

$$y_r^{out}(x)=\frac{y_r^0+W_r+y_c^0+W_c}{2}+\frac{(y_r^0+W_r)-(y_c^0+W_c)}{2}\sin\left(\frac{x-x_0}{L}\pi+\frac{\pi}{2}\right). \tag{11}$$

The transverse positions of the inner boundaries for $x_0<x<x_0+L_{lr}$ are given by

$$y_r^{in}(x)=\sqrt{\frac{W_0^2}{4}-(x-x_0)^2},$$

$$y_l^{in}(x)=-y_r^{in}(x). \tag{12}$$

We note that, as can be seen in Fig. 2, all the boundaries vary smoothly in the model. Thus, it can be assumed that scatterings by boundary roughness and by impurities are not present in the modeled devices.

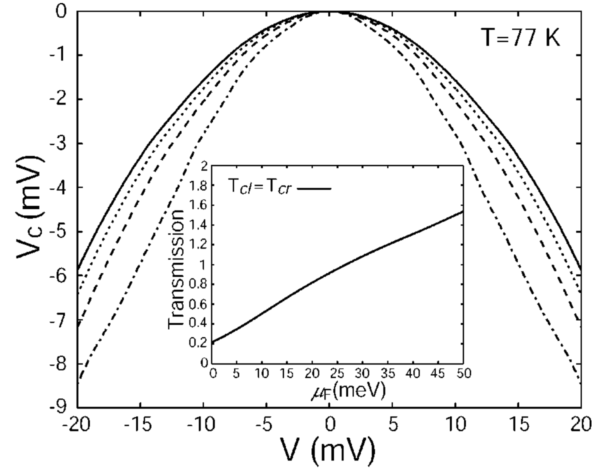

FIG. 3. V_c vs V for a symmetric TBJ with the parameters $W_l=W_r=70$ nm, $W_c=50$ nm, $W_0=92$ nm, $L_c=100$ nm, and $L_{lr}=46$ nm, calculated at $T=77$ K. The different curves correspond to $\mu_F=7$ meV (dashed-dotted line), $\mu_F=15$ meV (dashed line), $\mu_F=18.5$ meV (dotted line), and $\mu_F=21$ meV (solid line). Inset shows the transmission $T_{cl}(\mu_F,T)$ at $T=77$ K.

B. High-temperature transport

In Fig. 3, the calculated output voltage V_c as a function of applied bias voltage V at $T=77$ K, is shown for a symmetric TBJ with the geometrical parameters $W_l=W_r=70$ nm, $W_c=50$ nm, $W_0=92$ nm, $L_c=100$ nm, and $L_{lr}=46$ nm. The different curves correspond to different values of the chemical potential μ_F. We also show the corresponding transmission $T_{cl}(\mu_F,T)$ between the left and central leads, calculated at $T=77$ K, in the inset of the figure.

The following observations can be made from the results of Fig. 3. First of all, the output voltage V_c is negative for all finite values of $|V|$. Second, in general, the dependence is paraboliclike, in particular, at small values of $|V|$. Third, with the decrease of μ_F, the absolute value of the curvature of the parabolic behavior increases. These observations are in perfect agreement with the ones made in Refs. 7–10 and can be explained by the same arguments as those given in Ref. 7. For completeness and for further discussions, we briefly recall the main results of Ref. 7.

It was shown, in general, in Ref. 7 that in the limit of small bias $|V|$, the output voltage of a symmetric TBJ device operated in the push-pull fashion is given by

$$V_c=-\frac{1}{2}\alpha V^2+O(V^4), \tag{13}$$

where

$$\alpha=e\frac{\partial T_{cl}(\mu_F,T)/\partial\mu_F}{T_{cl}(\mu_F,T)}. \tag{14}$$

The above equations show that the sign of the output voltage V_c, from the central branch, at small bias depends on the slope of the transmission, $\partial T_{cl}(\mu_F,T)/\partial\mu_F$: a positive (negative) slope gives a negative (positive) output voltage V_c at small bias. Since, the transmission, $T_{cl}(\mu_F,T)$ is a mono-

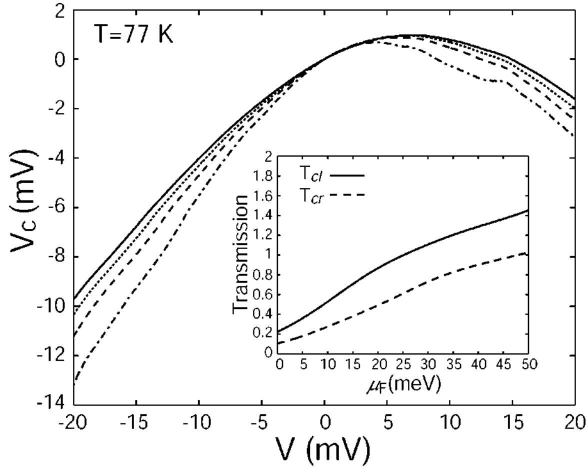

FIG. 4. V_c vs V for an asymmetric TBJ with the parameters $W_l=70$ nm, $W_r=40$ nm, $W_c=50$ nm, $W_0=92$ nm, $L_c=100$ nm, and $L_{lr}=46$ nm, calculated at $T=77$ K. Different curves correspond to $\mu_F=7$ meV (dashed-dotted line), $\mu_F=15$ meV (dashed line), $\mu_F=18.5$ meV (dotted line), and $\mu_F=21$ meV (solid line). Inset shows the transmission $T_{cl}(\mu_F,T)$ [solid line] and $T_{cr}(\mu_F,T)$ [dashed line] at $T=77$ K.

tonically increasing function of μ_F at $T=77$ K (inset of Fig. 3), the behavior at small bias voltages is negative and quadratically dependent on V, as predicted by Eq. (13). Furthermore, since the transmission is approximately a linear function of μ_F, the coefficient α depends approximately on μ_F according to $\alpha=e/\mu_F$. Thus, if the chemical potential is increasing, the coefficient α is decreasing, yielding smaller negative curvature of the V_c vs V curve, which is consistent with the behavior observed in Fig. 3.

In order to understand the V_c-V characteristics at large bias voltages, it is interesting to consider the zero-temperature equation

$$\int_{\mu_l}^{\mu_c} T_{cl}(\varepsilon)d\varepsilon=\int_{\mu_c}^{\mu_r} T_{rl}(\varepsilon)d\varepsilon, \tag{15}$$

which can be obtained from Eq. (10), by requiring $I_c=0$. In this case, for a symmetric TBJ, for which $T_{cl}(\varepsilon)=T_{rl}(\varepsilon)$, the electrochemical potential in the central probe, μ_c, will always remain at a value above the average of μ_l and μ_r if the transmissions $T_{cl}(\varepsilon)$ and $T_{rl}(\varepsilon)$ are increasing functions of energy. Hence, $\mu_c>\mu_F$ and V_c is negative and monotonically decreasing with the increase of the absolute value of the applied voltage, $|V|$. Although the results of Fig. 3 are calculated at $T=77$ K, similar arguments based on the increasing transmission functions $T_{cl}(\varepsilon)$ and $T_{rl}(\varepsilon)$ at this temperature explain the large-bias behavior observed in Fig. 3.

We have also calculated the V_c vs V dependence at $T=77$ K of an asymmetric TBJ, for which the width of the right branch has been decreased to $W_r=40$ nm (all other parameters are identical to the ones for the structure studied in Fig. 3). The results are shown in Fig. 4 along with the corresponding transmissions $T_{cl}(\mu_F,T)$ (solid line) and $T_{cr}(\mu_F,T)$ (dashed line) shown in the inset.

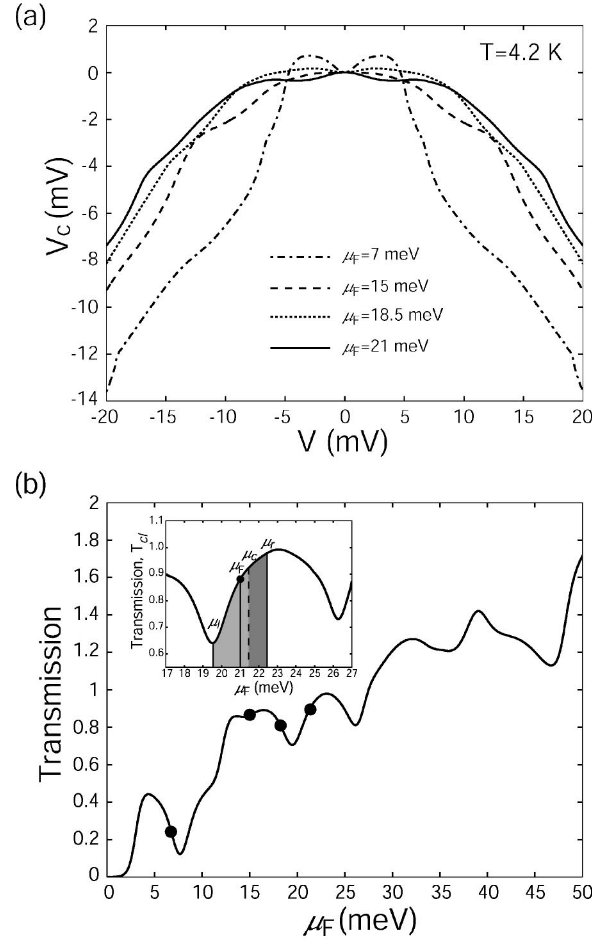

FIG. 5. (a) V_c vs V for the symmetric TBJ studied in Fig. 3 with the parameters $W_l=W_r=70$ nm, $W_c=50$ nm, $W_0=92$ nm, $L_c=100$ nm, and $L_{lr}=46$ nm, calculated at $T=4.2$ K. The different curves correspond to different values of μ_F. (b) Transmission $T_{cl}(\mu_F,T)$ at $T=4.2$ K. The black dots indicate values of μ_F at which the curves in Fig. 5(a) are calculated. Inset shows a blow up of the region in the $T_{cl}(\mu_F,T)$ curve around $\mu_F=21$ meV. Shaded areas illustrate the integration windows of the integrals on the left-hand side and right-hand side of Eq. (15) in the text. Note that $T_{cl}(\mu_F,T)=T_{cr}(\mu_F,T)$.

The results show that the output voltage V_c remains a paraboliclike function of V with a curvature that depends on μ_F in a similar way to that found for the symmetric device. However, V_c is no longer a symmetric function of V with respect to $V=0$, and can be positive at small values of V. The observed behavior again agrees perfectly with earlier theoretical predictions[7] and experimental observations.[9] The origin of the asymmetry is the difference in the transmissions between the left and the central branches and between the right and the central branches (seen in the inset of Fig. 4).

C. Low-temperature limit

We now consider the low-temperature transport properties of the TBJs studied in Sec. III B. In Fig. 5, we show the results calculated at $T=4.2$ K for the symmetric TBJ previously studied at $T=77$ K in Fig. 3. In Fig. 5(a), the V_c vs V

dependences, calculated at the same values of μ_F as previously used in Fig. 3, are shown. It is seen that overall the V_c versus V curves are symmetric with respect to $V=0$ and are bending toward negative values of V_c at large values of $|V|$. This is the same behavior as found in Fig. 3 and in previous calculations[7] and measurements.[8–10] However, it is also seen in Fig. 5(a) that the V_c vs V curves display slow oscillations and, depending on the chemical potential μ_F, can assume both negative and positive values at small bias voltages. These oscillatory and low-bias behaviors were not visible in the previously shown high-temperature results, neither were they observed in the experiments of Refs. 8–10 and the calculations of Ref. 7.

The above oscillatory and low-bias behaviors are signatures of quantum effects and can be explained using the characteristics of the calculated transmission $T_{cl}(\mu_F,T)$ at $T=4.2$ K, shown in Fig. 5(b). There, it is seen that the transmission exhibits a rich structure of dips, of varying amplitudes and widths. Similar dip structures and fluctuations have been previously found in the two-terminal conductance of a quantum channel with embedded cavities[18–20,28] and the multiterminal resistance of a four-terminal junction.[29] Associated with these dips in $T_{cl}(\mu_F,T)$, peaks are seen in the calculated transmission $T_{rl}(\mu_F,T)$ as well as in the reflection $R_{ll}(\mu_F,T)$ (not shown here). As shown for two-terminal cavity structures,[18–20,28] as well as for four-terminal junctions,[29] the rich dip structure seen in $T_{cl}(\mu_F,T)$ originates from antiresonant scattering of the electrons by quasibound states formed in the junction cavity region, and is a signature of quantum effects. Thus the number and energy position of the dips seen in $T_{cl}(\mu_F,T)$ depend sensitively on the structure of the cavity in the TBJ device.

The irregular and nonmonotonic dependence of $T_{cl}(\mu_F,T)$ on μ_F affects the push-pull operation of the TBJ in the following way. At small bias, it was shown in Sec. III B [Eq. (13)] that the sign of the output voltage V_c from the central branch depends on the slope of the transmission, $\partial T_{cl}(\mu_F,T)/\partial\mu_F$. Thus, a positive (negative, zero) slope gives a negative (positive, zero) output voltage V_c. Due to the fluctuating transmission characteristics [Fig. 5(b)], the slope of the transmission $T_{cl}(\mu_F,T)$ can be negative, zero, or positive, depending on the value of μ_F, and hence, the output voltage in turn is sensitive to the chemical potential of the TBJ. As an example, consider the transmission of Fig. 5(b) at values of μ_F (marked by black dots for clarity) at which the curves in Fig. 5(a) have been calculated. At the values of $\mu_F=7$ meV and $\mu_F=18.5$ meV, evidently $\partial T_{cl}(\mu_F,T)/\partial\mu_F$ is negative and, hence the output voltage V_c is positive at small bias [see dashed-dotted and dotted lines in Fig. 5(a)]. On the other hand, for $\mu_F=15$ meV and $\mu_F=21$ meV, the transmission slope is approximately zero and positive, respectively, correspondingly yielding a close to zero and negative V_c [dashed and solid curves in Fig. 5(a)] at small bias.

We now turn to the explanation of the general oscillatory behavior of the TBJ devices seen in a large range of bias voltage. At zero temperature, the condition, in which the output voltage V_c from the central branch of a symmetric TBJ device is determined, is given by Eq. (15) (this is a fairly good approximation at $T=4.2$ K as well since the thermal energy, $k_BT\ll 1$ meV). Consider now the inset of Fig. 5(b) which shows a blow-up of the region around $\mu_F=21$ meV [a value at which the V_c-V curve corresponding to the solid line in Fig. 5(a) was calculated]. The two shaded areas in the inset mark the two integration regions on the left- and right-hand sides of Eq. (15). For the specific bias situation depicted in the inset ($V\approx 3$ mV), the transmission probability in the energy range $19.5<\mu_F<22.5$ meV, accessible to electrons at the given bias voltage, is an increasing function of energy and thus, in order for current balance to be achieved μ_c has to take on a value above the average of μ_l and μ_r (see the inset), hence $\mu_c>\mu_F$ yielding a negative V_c. By increasing the value of the bias voltage from zero, V_c decreases monotonically as long as both μ_l and μ_r remain on the upward slope of the transmission curve [inset of Fig. 5(b)]. As V continues to increase, and thus effectively increasing the energy range for which electrons are transmitted across the TBJ, V_c turns to increase at a bias voltage around $V\approx 3.5$ mV. This is due to the fact that as V is further increased, the electron transmission probability between the central and the left leads increases [see the energy interval $17<\mu_F<19$ meV on the low-energy side in the inset of Fig. 5(b)] whereas the electron transmission probability between the right and the central leads correspondingly decreases [see the energy interval $23<\mu_F<26$ meV on the high-enegry side in the inset of Fig. 5(b)], which effectively lowers the electrochemical potential μ_c at the central lead towards the value of μ_l. By further increasing the bias voltage, V_c continues to decrease due to the overall increasing transmission function. However, due to the fluctuating nature of the transmissions as a function of μ_F, V_c displays corresponding fluctuations with variations of the bias voltage which can be understood by the previously given arguments. The behavior of the remaining curves in Fig. 5(a) can be explained in a similar fashion.

We have performed similar low-temperature calculations for the asymmetric TBJ, previously studied in Fig. 4 at $T=77$ K. The transport characteristics, calculated at $T=4.2$ K, are shown in Fig. 6. In Fig. 6(a), the V_c vs V dependence, calculated at the same values of μ_F as in Fig. 4, is shown. In addition, we also show the transmissions $T_{cl}(\mu_F,T)$ (solid line) and $T_{cr}(\mu_F,T)$ (dashed line) in Fig. 6(b). The thin, solid vertical lines mark values of μ_F at which the curves in Fig. 6(a) are calculated.

In addition to the asymmetry, already observed and discussed at high temperatures, the same types of oscillations, which were seen in the low-temperature transport characteristics of the symmetric TBJ shown in Fig. 5, are seen to occur, both in the transmissions and the V_c vs V curves. Again, the origin of the observed deviations from the high-temperature behavior is due to the scattering of electrons from quasibound states formed in the cavitylike coupling window between the three arms of the TBJ. As shown in Fig. 6(b), the transmissions T_{cl} and T_{rl} exhibit strong fluctuations due to the complex scatterings, giving rise to the oscillations observed in the calculated V_c vs V dependences. Recently, such type of oscillations have been observed in the low-

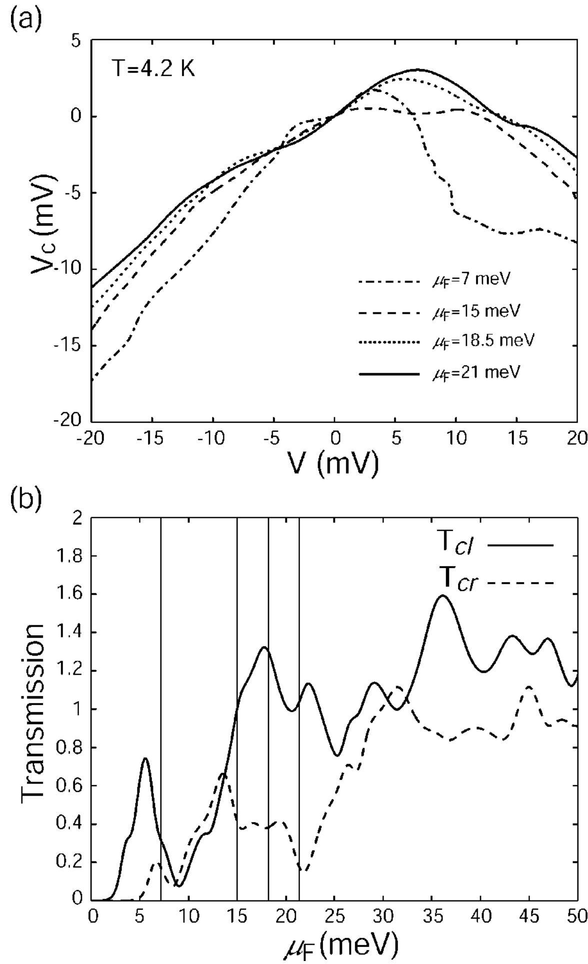

FIG. 6. (a) V_c vs V for the asymmetric TBJ studied in Fig. 4 with the parameters $W_l = 70$ nm, $W_r = 40$ nm, $W_c = 50$ nm, $W_0 = 92$ nm, $L_c = 100$ nm, and $L_{lr} = 46$ nm, calculated at $T = 4.2$ K. The different curves correspond to different values of μ_F. (b) Transmission $T_{cl}(\mu_F, T)$ [solid line] and $T_{cr}(\mu_F, T)$ [dashed line] at $T = 4.2$ K. The vertical lines mark values of μ_F at which the curves in (a) are calculated.

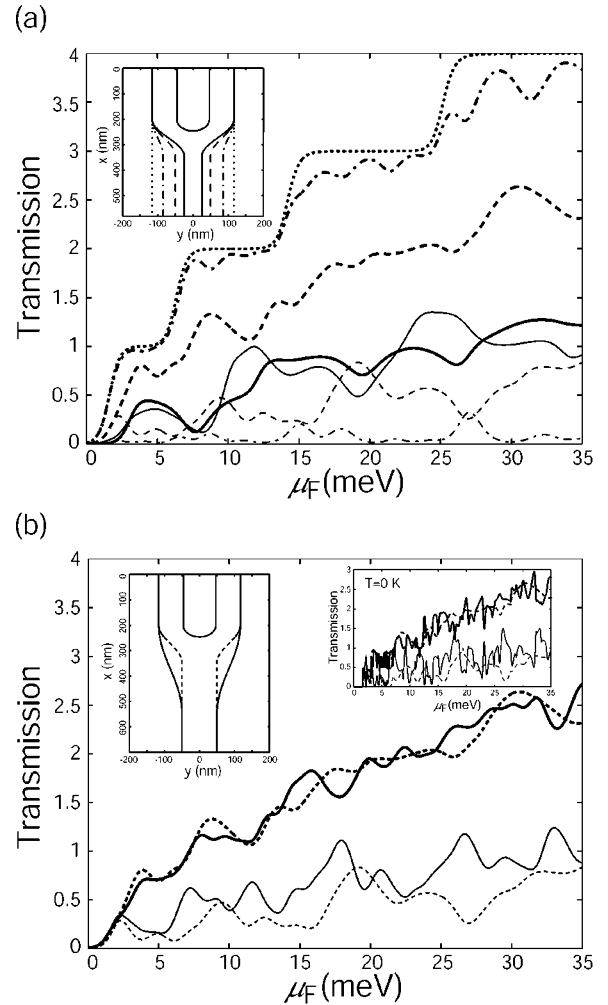

FIG. 7. Transmission characteristics for TBJs with the parameters $W_l = W_r = 70$ nm, $W_0 = 92$ nm, and $L_{lr} = 46$, calculated at $T = 4.2$ K. (a) Transmissions $T_{cl}(\mu_F, T)$ and $T_{rl}(\mu_F, T)$ for four TBJ structures with $L_c = 100$ nm. The different curves correspond to structures with $W_c = 50$ nm [solid lines], 100 nm [dashed lines], 170 nm [dashed-dotted lines], and 232 nm [dotted lines]. The thick lines correspond to the transmission $T_{cl}(\mu_F, T)$ and the thin lines to $T_{rl}(\mu_F, T)$. Inset shows the geometries of the four TBJs. (b) Transmissions $T_{cl}(\mu_F, T)$ [thick lines] and $T_{rl}(\mu_F, T)$ [thin lines] for two TBJs with $W_c = 100$ nm. The solid lines correspond to a TBJ with $L_c = 300$ nm. The dotted lines correspond to a TBJ with $L_c = 100$ nm. Left inset shows the geometries and dimensions of the two structures. Right inset shows the transmissions $T_{cl}(\mu_F, T)$ and $T_{rl}(\mu_F, T)$ calculated at $T = 0$ K. [Note that for all structures $T_{cl} = T_{lc} = T_{rc} = T_{cr}$ and $T_{lr} = T_{rl}$.]

temperature V_c vs V dependence of T-shaped TBJs based on high-electron-mobility GaInAs/InP quantum-well structures[30] (the high-temperature measurements of the same devices were previously shown in Ref. 9).

D. Low-temperature transmission fluctuations

Due to their quantum-mechanical origin, the fluctuations observed in the low-temperature output voltage $V_c(V)$, as well as the transmissions between the three arms of the TBJ, should be strongly dependent on the detailed geometry and structure of the device. To show this, we have investigated several TBJs with different shapes and sizes of the central coupling region as well as of the three branches. We have found that the generic features discussed in Figs. 5 and 6 are observable for a wide range of TBJ geometries provided a cavity is formed at the junction between the three leads.

The influence of a cavity at the central junction region is exemplified in Fig. 7 where we show the calculated transmissions $T_{cl}(\mu_F, T)$ and $T_{rl}(\mu_F, T)$ for several symmetric TBJs at $T = 4.2$ K [note that $T_{cl} = T_{lc} = T_{rc} = T_{cr}$ and the same discussion applies for electrons incident from the right and central leads]. All geometrical parameters but W_c and L_c are identical to the ones used in the TBJ studied in Figs. 3 and 5. In Fig. 7(a), $L_c = 100$ nm [fixed to the value previously used in Figs. 3 and 5] and $W_c = 50, 100, 170$, and 232 nm. For the TBJ with $W_c = 232$ nm, $y_l^{out}(x) = y_l^0 = y_c^0$ and $y_r^{out}(x) = y_r^0 + W_r$ [Eq. (11)] and thus, the transverse position of the outer boundaries of the TBJ is constant along the x direction of

transport [see dotted lines in the inset of Fig. 7(a)]. Hence, no cavity is formed at the junction between the three branches. The dotted line in Fig. 7(a), showing $T_{cl}(\mu_F,T)$, shows that the transmission increases in perfect unit steps, corresponding to the successive opening of one-dimensional subbands in the leads. Since $W_c \gg W_{l,r}$ in this case, the transmission is limited by the number of open modes in the left/right leads at a given value of μ_F yielding the observed unit transmission steps whenever a new transverse mode in the left/right lead falls below μ_F. In contrast, for W_c comparable to or smaller than W_l and W_r, the transport (transmission) is limited by the number of modes open for conduction in the central lead. Consequently, for such a device, in the absence of scattering, the transmission T_{cl} increases in half-unit steps whenever a new mode is opened in the central lead, as a result of electron waves incident from the central branch being equally divided between the left and the right branches of the symmetric TBJ. Naturally, for an asymmetric TBJ, the corresponding transmission spectra of T_{cl} would consist of half-unit and unit steps at values of μ_F at which a new mode is opened in any one of the three leads. All these features have been verified in our calculations (not shown here).

As W_c is gradually decreased, a cavitylike structure is formed at the junction between the three branches of the TBJ [see the inset of Fig. 7(a)]. The thick lines show the transmission $T_{cl}(\mu_F,T)$ for the TBJs with $W_c=170$ nm (dashed-dotted line), $W_c=100$ nm (dashed line) and $W_c=50$ nm (solid line). In addition, the thin lines display the corresponding transmission $T_{rl}(\mu_F,T)$ for the same structures. With the decrease of W_c, in general, the transmission $T_{cl}(\mu_F,T)$ is seen to decrease gradually, partly due to the decrease in the number of available subbands in the central lead. More important, the formation of a cavity at the central junction region provides a source of scattering for incident electrons enabling reflection of electrons into, in this case, the left lead (not shown here), as well as transmission of electrons to the right lead, which is seen in the transmission curves $T_{rl}(\mu_F,T)$. Furthermore, distinct and irregular fluctuations are also observed in the transmissions of the TBJ devices in the presence of a cavity in the central junction region. These fluctuations are caused by the scattering of incident electrons by quasibound states formed in the cavity region.

In Fig. 7(b), the transmissions of two symmetric TBJs with $W_l=W_r=70$ nm and $W_c=100$ nm are shown for two different lengths (and effectively also shapes) of the central junction. The solid lines represent the transmissions $T_{cl}(\mu_F,T)$ (thick solid line) and $T_{rl}(\mu_F,T)$ (thin solid line) of a TBJ with 300-nm-long junction region ($L_c=300$ nm), see the left inset of Fig. 7(b). For comparison, the corresponding results for a TBJ with $L_c=100$ nm [previously shown in Fig. 7(a)] are shown as dotted lines [see the left inset of Fig. 7(b) for geometrical comparison between the two structures]. It is seen that, in comparison, more periods of fluctuations are observed in the transmissions of the TBJ with the larger junction region. In particular, at even lower temperatures [see the right inset of Fig. 7(b)], the transmission is found to exhibit rapid (short-period) fluctuations, which are rapidly smeared out already at $T=4.2$ K at which the transmissions in Fig. 7 are calculated. This is consistent with the picture that, as the area of the junction cavity is increased, the quasibound level structure becomes more dense.

TABLE I. Truth tables for logic (a) AND and (b) OR gates. Due to their inherent nonlinear electrical properties, TBJs can function as logic gates.

AND (a)			OR (b)		
Input		Output	Input		Output
V_l	V_r	V_c	V_l	V_r	V_c
0	0	0	0	0	0
0	1	0	0	1	1
1	0	0	1	0	1
1	1	1	1	1	1

E. Logic functionality

It has been previously proposed that due to the inherent nonlinear electrical properties of TBJs, a single TBJ device could be used as a logic gate.[7,13,14] For example, when dc voltages V_l and V_r are applied to the left and right branches of a symmetric TBJ device, the output voltage V_c can be positive (a binary value of 1) only when both of the applied dc voltages are positive. Thus, the device operates as a logic AND gate [Table I(a)]. However, the device may also be used as a logic OR gate if the negative output voltage V_c is taken as the binary value of 1 [Table I(b)].

The proposals of Refs. 7,13,14 were made for symmetric, adiabatic TBJs where V_c only assumes negative values during the push-pull operation. However, as shown in Sec. III C, the output voltage V_c may assume both negative *and* positive values at low temperatures for symmetric TBJs if quantum-mechanical scattering in the junction region is taken into account. It was also shown that the sign and amplitude of V_c is strongly dependent on the chemical potential μ_F due to the fluctuations in the transmissions $T_{cl}(\mu_F,T)$ and $T_{cr}(\mu_F,T)$ caused by electron scattering at the junction between the three arms of the TBJ. Hence, in an experimental situation, the sign and amplitude of V_c may be controlled, e.g., by means of a gate situated on top of the TBJ structure, thereby enabling multilogic functionality. By changing a voltage applied to the gate such that μ_F is in a range for which V_c only assumes negative values, the TBJ functions as a logic AND gate (provided $V_c>0$ is defined as binary 1). Correspondingly, if the voltage applied to the gate is varied such that μ_F is in a range where V_c only assumes positive values at a given value of $|V|$, the TBJ functions as a logic OR gate .

In Fig. 8, the output voltage V_c, calculated at $T=4.2$ K, is shown as a function of μ_F for three bias voltages for the symmetric TBJ studied in Figs. 3 and 5. Clear and well-defined regions, in which the output voltage V_c is negative or positive, are seen in the three curves calculated for different values of $|V|$. Hence, the multilogic functionality previously mentioned applies for this TBJ. In the intervals of μ_F denoted by I, III, V, and VII, V_c is mainly negative and thus the

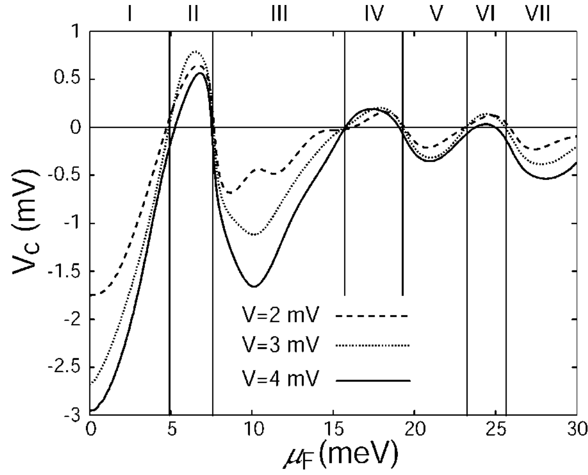

FIG. 8. Output voltage V_c as a function of μ_F at $T=4.2$ K for the TBJ previously studied in Figs. 3 and 5 with parameters $W_l=W_r=70$ nm, $W_c=50$ nm, $W_0=92$ nm, $L_c=100$ nm, and $L_{lr}=46$ nm. The different curves correspond to different values of V as shown in the figure.

TBJ functions as a logic AND gate [Table I(a)] (again defining positive values of V_c as binary 1). In contrast, in the intervals of μ_F denoted by II, IV, and VI, V_c displays positive values and thus the functionality of the TBJ complies with the logic OR truth table shown in Table I(b). We have analyzed several other TBJ structures with different geometries and sizes and found similar results, provided that a cavity is present at the central junction region. Naturally, due to the quantum nature of the observed effects, the observed characteristics are very sensitive to the detailed structure of the TBJ.

IV. SUMMARY AND CONCLUDING REMARKS

In this paper, we have shown that based on the ballistic and quantum-mechanical nature of the electron transport, TBJs exhibit interesting transport characteristics. Using a formalism based on a scattering-matrix approach[22] and the Landauer-Büttiker theory of transport,[11] we have performed numerical calculations for TBJ structures with different structural properties, at both high and low temperatures as well as for small and large applied bias voltages.

In the nonlinear regime of transport, the push-pull operation of a TBJ yields strong nonlinearities in the output voltage V_c at the central branch of the device. At high temperatures, the symmetric TBJ devices, when operated in the push-pull fashion, exhibit the same electrical characteristics as in Refs. 7–10, i.e., negative output voltage V_c for all finite values of $|V|$ as well as a paraboliclike dependence on V at the limit of small-bias voltage. We have found that these high-temperature characteristics are qualitatively insensitive to the structural details of the devices and reveal little effect of quantum scattering. Thus, our results support the assumptions made in Ref. 7.

In contrast, at low temperatures, we have found that V_c exhibits slow fluctuations, and can assume either negative or positive values at small bias regions, depending on the chemical potential. These behaviors have been explained in terms of the fluctuations seen in the transmissions $T_{cl}(\mu_F,T)$ and $T_{cr}(\mu_F,T)$ and are signatures of quantum effects. We have examined the transmissions for several TBJs and have concluded that the origin of the observed transmission fluctuations is the electron scattering in the junction region between the three branches of the TBJ, where a cavity can form. Due to the quantum-mechanical nature of the scattering, the transmission fluctuations are found to be very sensitive to the size and shape of the cavity, as well as the position and size of the connecting branches.

We emphasize that the two main characteristic features of the TBJs studied in this paper, i.e., the nonlinear electrical behavior, and the fluctuations in the transmissions and the sign of the output voltage V_c, are based on two different mechanisms, the ballistic nature of the electron transport and quantum interference, respectively. The overall nonlinear behavior of the V_c vs V dependence has been found, in agreement with experiments,[9] to be robust even at room temperature, as long as the mean-free path of the system is larger than the device size [note that it has been shown experimentally that the mean-free path of electrons in III–V semiconductor heterostructures can be of the order of 100 nm at room temperature and a few μm at 300 mK (Ref. 9)]. The quantum interference effects on the other hand are far more sensitive to temperature and vanish already at moderately low temperatures, due to the decrease of the phase-coherence length with increase of temperature, caused by electron-phonon and electron-electron scattering, and the thermal smearing originating from the terms $f(\varepsilon-\mu_i,T)$ and $-\partial f(\varepsilon-\mu_F,T)/\partial\varepsilon$ in Eqs. (10) and (9). In our calculations, all quantum interference effects for the structures studied in this paper disappear due to thermal smearing already at $T=30$ K. However, for structures small enough compared to the phase-coherence length and with quasibound level spacings larger than the thermal energy k_BT, the quantum effects reported in this paper are expected to be observable at high temperatures.

Finally, we have proposed and demonstrated that based on the low-temperature characteristics found in Sec. III C, a single TBJ device can function as an extremely compact multilogic gate, the functionality of which may be tuned by means of a gate. We believe that the observed quantum effects at low temperatures may be observable and significant also for other types of three-terminal junction structures based on, e.g., single molecules or carbon nanotubes,[31] in which the quantization effects may be large enough to permit high-temperature operation.

ACKNOWLEDGMENTS

This work was supported by the Swedish Foundation for Strategic Research (SSF) and the Swedish Research Council (VR) and by the European Commission through the Information Society Technologies (IST) Program Project NEAR. Furthermore, the authors would like to thank Ivan Shorubalko for sharing of experimental results prior to publication.

*Electronic mail: Dan.Csontos@ftf.lth.se
†Electronic mail: Hongqi.Xu@ftf.lth.se

[1] J.A. del Alamo and C.C. Eugster, Appl. Phys. Lett. **56**, 78 (1990).
[2] F. Sols, M. Macucci, U. Ravaioli, and K. Hess, J. Appl. Phys. **66**, 3892 (1989).
[3] T. Palm and L. Thylén, Appl. Phys. Lett. **60**, 237 (1992).
[4] T. Palm, Phys. Rev. B **52**, 13 773 (1995).
[5] L. Worschech, B. Weidner, S. Reitzenstein, and A. Forchel, Appl. Phys. Lett. **78**, 3325 (2001).
[6] L. Worschech, S. Reitzenstein, M. Keßelring, A. Schliemann, and A. Forchel, Physica E (Amsterdam) **12**, 688 (2002).
[7] H.Q. Xu, Appl. Phys. Lett. **78**, 2064 (2001).
[8] K. Hieke and M. Ulfward, Phys. Rev. B **62**, 16 727 (2000).
[9] I. Shorubalko, H.Q. Xu, I. Maximov, P. Omling, L. Samuelson, and W. Seifert, Appl. Phys. Lett. **79**, 1384 (2001).
[10] L. Worschech, H.Q. Xu, A. Forchel, and L. Samuelson, Appl. Phys. Lett. **79**, 3287 (2001).
[11] M. Büttiker, Phys. Rev. Lett. **57**, 1761 (1986).
[12] M. Büttiker, Phys. Rev. B **41**, 7906 (1990).
[13] H.Q. Xu, Appl. Phys. Lett. **80**, 853 (2002).
[14] H.Q. Xu, Physica E (Amsterdam) **13**, 942 (2002).
[15] I. Shorubalko, H.Q. Xu, I. Maximov, D. Nilsson, P. Omling, L. Samuelson, and W. Seifert, IEEE Electron Device Lett. **23**, 377 (2002).
[16] I. Maximov, P. Carlberg, D. Wallin, I. Shorubalko, W. Seifert, H.Q. Xu, L. Montelius, and L. Samuelson, Nanotechnology **13**, 666 (2002).
[17] D. Csontos and H.Q. Xu, Appl. Phys. Lett. **77**, 2364 (2000).
[18] K. Nakazato and R.J. Blaikie, J. Phys.: Condens. Matter **3**, 5729 (1991).
[19] H. Kasai, K. Mitsutake, and A. Okiji, J. Phys. Soc. Jpn. **60**, 1679 (1991); H. Ishio and K. Nakamura, *ibid.* **61**, 2649 (1992).
[20] S. Yuan and B. Gu, Z. Phys. B: Condens. Matter **92**, 47 (1993).
[21] H. Linke, W. Sheng, A. Löfgren, H.Q. Xu, P. Omling, and P.E. Lindelof, Europhys. Lett. **44**, 341 (1998).
[22] D. Csontos and H.Q. Xu, J. Phys.: Condens. Matter **14**, 12 513 (2002).
[23] M. Cahay, S. Bandyopadhyay, and H.R. Frohne, J. Vac. Sci. Technol. B **8**, 1399 (1990).
[24] H.Q. Xu, Phys. Rev. B **50**, 8469 (1994).
[25] W. Sheng, J. Phys.: Condens. Matter **9**, 8369 (1997).
[26] H. Mizuta, Microelectron. J. **30**, 1007 (1999).
[27] H.Q. Xu, Phys. Rev. B **47**, 15 630 (1993).
[28] H.Q. Xu and W.D. Sheng, Phys. Rev. B **57**, 11 903 (1998).
[29] D.G. Ravenhall, H.W. Wyld, and R.L. Schult, Phys. Rev. Lett. **62**, 1780 (1989).
[30] I. Shorubalko (private communication).
[31] J. Li, C. Papadopoulos, and J. Xu, Nature (London) **402**, 254 (1999); C. Papadopoulos, A. Rakitin, J. Li, A.S. Vedeneev, and J.M. Xu, Phys. Rev. Lett. **85**, 3476 (2000); B.C. Satishkumar, P.J. Thomas, A. Govindaraj, and C.N.R. Rao, Appl. Phys. Lett. **77**, 2530 (2000); W.Z. Li, J.G. Wen, and Z.F. Ren, *ibid.* **79**, 1879 (2001).